Engineering and Applied Science Research 2024;51(1):22-33 Research Article

Engineering and Applied Science Research

https://www.tci-thaijo.org/index.php/easr/index

Published by the Faculty of Engineering, Khon Kaen University, Thailand

Comparative study on material models for BS 080M46 medium carbon steel

Nattarawee Siripath[1], Surasak Suranuntchai*[1] and Sedthawatt Sucharitpwatskul[2]

[1]Department of Tool and Materials Engineering, Faculty of Engineering, King Mongkut's University of Technology, Bangkok 10140, Thailand
[2]National Science and Technology Development Agency (NSTDA), Thailand Science Park, Pathum Thani 12120, Thailand

Received 7 July 2023
Revised 20 October 2023
Accepted 6 November 2023

Abstract

This work focused on studying the flow behavior of BS 080M46 medium carbon steel through hot compression tests, covering a deformation temperature of 900, 1000, 1100, and 1200°C and strain rates varying from 0.1 to 10 s^{-1}. The purpose of this work was to effectively predict the flow behavior of the material at elevated temperatures using two different constitutive models: the Arrhenius-based and the Hansel-Spittel model. The application of the regression method involved fitting the experimental stress-strain data to obtain the material constants for these models. A comparison was made between the experimental and predicted flow stresses based on the two constitutive models, demonstrating a strong correlation with the experimental data. The developed Arrhenius-based constitutive model exhibited greater accuracy and reliability in its predictability compared to the Hansel-Spittel constitutive model, with *AARE* of 7.5231%, an *RMS* of 7.3565 MPa, and an *R* value of 0.98450. To further validate the predictive capability of the two constitutive models, they were incorporated into finite element software to conduct simulations of the hot compression tests. Comparing the actual load-displacement curves with those obtained curves obtained through finite element simulations revealed a comparable consistency between the predicted and actual load-displacement curves.

Keywords: Finite element modeling, BS 080M46 medium carbon steel, Hansel-Spittel constitutive model, Zener-Hollomon parameters, Arrhenius-based constitutive model

1. Introduction

BS 080M46 is classified as medium carbon steel grade with excellent mechanical properties and ease of processing, making it appropriate for high-stress loads, wear resistance, and precision machining. It is widely used in machinery components such as gears, axles, crankshafts, connecting rods, base plates, springs, milling cutters, and stud shafts that require high precision, durability, and resistance to wear from various machining tools. The machinery components typically experience extensive strain, strain rate, and temperature variations as part of the hot forming process [1].

Metal forming is a manufacturing process that involves the plastic deformation of a given material, typically with simple geometry, in order to achieve the required shape and dimensions. The primary factor shaping the quality of products in advanced manufacturing technologies such as forging, extrusion, and rolling is the plastic flow of metal at elevated temperatures. Typically, these processes are conducted at temperatures above the recrystallization point of the material [2, 3]. However, it is worth noting that the hot working process, despite its advantages, can be a time-consuming and costly endeavor. This is primarily due to the reliance on trial-and-error methods, which necessitate iterative adjustments and heavily depend on the expertise and experience of the designer or operator. As a result, the process can be inefficient, leading to increased production time and costs. To address these challenges, there is a growing need for more efficient and optimized approaches in hot working processes. By incorporating advanced techniques, such as computer simulations and numerical modeling, it is possible to reduce reliance on trial-and-error methods and enhance the predictability and accuracy of the hot working processes.

The mathematical description of the relationship between flow stress and deformation parameters can be achieved through the application of a constitutive model under various deformation conditions [4, 5]. The constitutive models are commonly used in FE software to facilitate the simulating the forming process [6]. They are used to represent the material flow behavior and aid in achieving more precise predictions, enabling better control and optimization of the hot working processes. In recent decades, researchers have made numerous attempts to utilize the regression method to establish constitutive relationships, such as the well-known Arrhenius-based and the Hansel-Spittel constitutive model. Their ability to incorporate the characteristic flow stress peak and subsequent material softening resulting from dynamic recrystallization makes them well-suited for describing the hot deformation behavior. The constitutive model for hot deformation which was presented by Sellars and McTegart [7] is gaining wide acceptance that used to characterize the material flow behavior. Sellars and Tegart introduced the Arrhenius hyperbolic constitutive model, which accurately depicts the correlation among flow stress, strain rate, and temperature. This model highlights the importance of thermal activation energy in controlling the hot deformation process. The hyperbolic sine, exponential, and power functions of the Arrhenius flow stress model are used on materials under varying stress levels. Since then, numerous scholars have successfully demonstrated the highly

*Corresponding author.
Email address: surasak.sur@kmutt.ac.th
doi: 10.14456/easr.2024.3

accurate predictability of the Arrhenius model in describing the high-temperature flow behavior of a variety of materials, including medium carbon steel [8], the alloys 2519 aluminum [9], SNCM8 [1], and Al-6.32Zn-2.10Mg [10], as well as the alloys Fe-21Cr-1.5Ni-5Mn [11]. Yin et al. [12] conducted a study on the thermal compressive deformational characteristics of GCr15 steel. In their research, they established a thermoplastic constitutive equation by combining the Arrhenius equation and the Zener-Hollomon parameter. The findings of the analysis demonstrated that the established constitutive equation yielded precise and consistent results. With a specialized focus on hot working, the Hansel-Spittel constitutive model provides a mathematical equation that comprehensively relates flow stress, strain, strain rate, and temperature. This model takes into consideration the influence of strain rate sensitivity, thereby providing a more thorough representation of material behavior [13]. This model consists of a set of nine parameters to accurately predict flow stress. It is widely utilized in Finite Element Method (FEM) simulations for simulating bulk metal forming processes [14-16]. The application of the Hansel-Spittel constitutive model has been observed in a wide range of materials. Liang et al. [6] introduces the Hansel-Spittel constitutive model, specifically designed for the HNi55-7-4-2 alloy, which incorporates stress-strain curves from a hot-compression test. It accurately predicts flow stress and load-displacement curves, aligning well with experimental results. The proposed model facilitates the computational analysis of hot precision forging for a synchronizer ring, successfully analyzing material flow and detecting manufactured defects. Chen's research focused on studying the flow behavior of different alloys under high-temperature plastic deformation. Through thermal simulation and employing constitutive models, Chen accurately predicted the thermal deformation behavior of Cr5 [15], X12 ferritic heat-resistant steel [16], Cr8 alloy steel [17], and Ti6Al4V alloy [18]. The research provided theoretical support for the development of hot-forming processes, numerical simulations, and optimization of hot forging parameters for these alloys. Furthermore, Chen established hot processing maps and identified microstructural features, enhancing the understanding and optimization of formability at elevated temperatures.

This work aimed to study the flow behavior of BS 080M46 medium carbon steel through a hot compression test, which was performed over a deformation temperature range of 900 to 1200°C, with strain rates of 0.1, 1, and 10 s^{-1}. To effectively predict the flow behavior under high temperatures, two different constitutive models, namely the Arrhenius-based and the Hansel-Spittel constitutive model, were employed. The material parameters of the constitutive models were determined by fitting the curves through the regression method. The numerically calculated stress-strain curves were subjected to a comparative analysis with the corresponding experimental curves, aiming to assess their predictability and accuracy using the product of three standard statistical parameters−average absolute relative error (*AARE*), root mean square (*RMS*) and correlation coefficient (*R*). Additionally, the load-displacement curves from the FE simulation were validated against the experimental data.

2. Material and experiment procedure

In this paper, the 080M46 medium carbon steel was investigated. The chemical composition of the steel was analyzed in terms of weight percentage (wt%) using an optical emission spectrometer (OES). The composition details are outlined in Table 1. A series of thermal compression experiments were performed utilizing a Baehr DIL-805 deformation dilatometer. The twelve cylindrical samples were prepared with a diameter of 5 millimeters and a height of 10 millimeters by laser cutting tool. The deformation temperature was directly detected by placing a thermocouple on the surface of the sample. The deformation condition parameters consisted of four temperatures (900, 1000, 1100, and 1200°C) and three different strain rates (0.1, 1, and 10 s^{-1}). Each sample was installed in a vacuum chamber filled with Argon gas. The provided sample was subjected to heating by an induction coil at a heating rate of 1.625°C per second, reaching the given temperatures. Following that, the sample was held at the given temperatures for a duration of 1 minute in order to ensure uniformity of temperature distribution throughout the sample. The sample was compressed to a height reduction of 60% using an Alumina punch and immediately quenched in the Argon gas until it reached room temperature at a cooling rate of 40°C per second. The deformation route of the hot compression experiment was displayed in Figure 1(a). The stress-strain data can be obtained by recording the applied load (L) and the change in length at regular intervals as the sample is compressed [2]. The flow stress (σ) and true strain (ε) are obtained using $\sigma = L/A$ and $\varepsilon = ln(h/h_0)$, respectively, A represents the instantaneous cross-sectional area, h_0 and h are initial and instantaneous heights, respectively. The flow curves corresponding to the various deformation conditions have been displayed in Figures 1(b) to 1(d).

Table 1 Chemical compositions of BS 080M46 medium carbon steel.

C	Si	Mn	P	S	Ni	Cr	Mo	Cu
0.4671	0.1940	0.6730	0.0265	0.0214	0.0682	0.1100	0.0155	0.1780

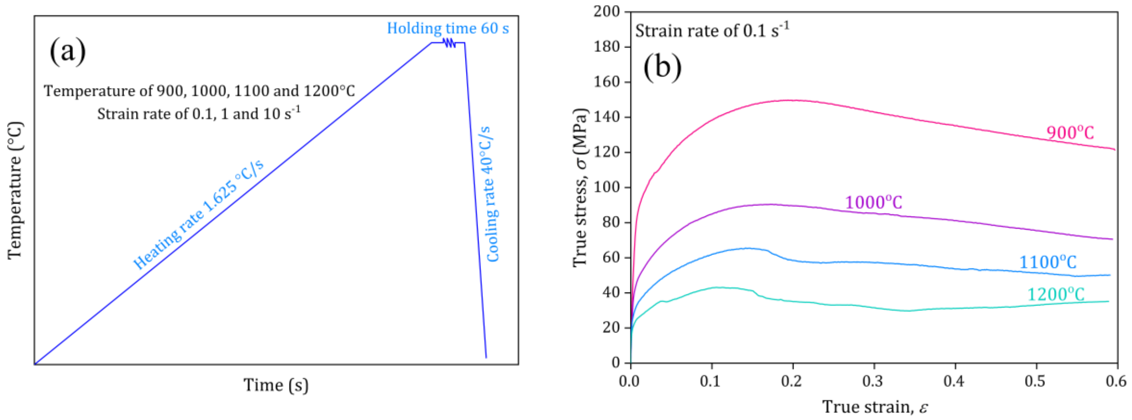

Figure 1 (a) Processing route of the hot compression experiment and the flow stress curves of BS 080M46 medium carbon steel under varying deformation temperatures at a strain rate of (b) 0.1 s^{-1}; (c) 1 s^{-1}; and (d) 10 s^{-1}

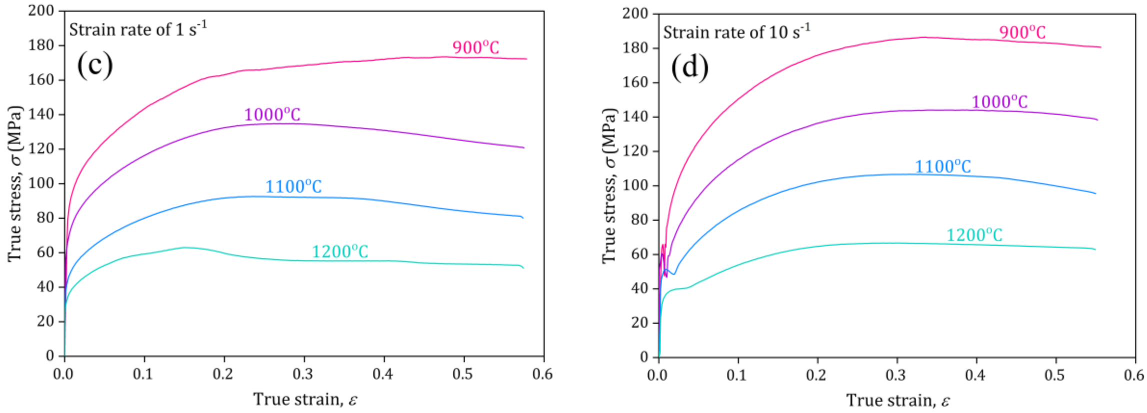

Figure 1 (continued) (a) Processing route of the hot compression experiment and the flow stress curves of BS 080M46 medium carbon steel under varying deformation temperatures at a strain rate of (b) 0.1 s^{-1}; (c) 1 s^{-1}; and (d) 10 s^{-1}

3. Developing the constitutive models of stress-strain behavior

3.1 Flow curves

Flow curves represent the stress-strain relationship under specific deformation conditions, often displaying dynamic recrystallization (DRX) behavior, characterized by an initial peak stress followed by a gradual decline to a state of steady stress. It is evident that flow stress is notably influenced by variations in deformation temperature and strain rate. The flow curves for various deformation temperatures at a strain rate of 0.1, 1, and 10 s^{-1} are respectively illustrated in Figures 1(b) to 1(d). At a certain strain rate, the deformation temperature decreases, and the flow stress tends to increase. Lowering the temperature of a material generally makes its atomic structure more stable and resistant to deformation resulting in a higher flow stress, which means more force is required to make the material deform or flow. In contrast to lower temperatures, higher temperatures generally decrease flow stress by increasing atomic mobility through greater thermal energy. This enhances ductility, aiding processes like hot forging and metal casting. Furthermore, under constant temperature deformations, a material subjected to a high strain rate usually shows increased flow stress due to limited time for dislocations to adjust, thereby making the material more resistant to deformation and less ductile. Conversely, at low strain rates, flow stress tends to decrease as the slower deformation rate allows dislocations more time to interact and results in reduced flow stress. As a result, lower temperatures and higher strain rates tend to increase flow stress, making materials more rigid and less ductile. Conversely, reducing the strain rate typically correlates with lower flow stress and enhanced level of ductility, making the material easier to deform.

3.2 Arrhenius-based constitutive model

The Arrhenius-based constitutive model is a material modeling approach that is utilized to depict the mechanical behavior of materials at elevated temperatures. The following expression relates the strain rate in heated forming to the flow stress, activation energy, and temperature:

$$\dot{\varepsilon} = AF(\sigma)\exp\left(-\frac{Q}{RT}\right) \tag{1}$$

In Eq. 1, $\dot{\varepsilon}$ denoted the strain rate in a unit of s^{-1}, A is a constant, $F(\sigma)$ is a function of stress which can be described by Eq. 2, Q is the activation energy for deformation expressed in kJ per mol), R represents the universal gas constant with a value of 8.314 $J{\cdot}mol^{-1}K^{-1}$, and T is the absolute temperature measure in Kelvin.

$$F(\sigma) = \begin{cases} \sigma^{\eta} & : \alpha\sigma < 0.8 \\ \exp(\beta\sigma) & : \alpha\sigma > 1.2 \\ [\sinh(\alpha\sigma)]^{n} & : \text{for all } \sigma \end{cases} \tag{2}$$

where η, β, $\alpha = \beta/\eta$ and n are apparent material constants [8-12, 19-24]. The rate of deformation at high temperatures is governed by the activation energy of the material, as described by the Zener-Hollomon parameter. A constitutive model that considers the influence of temperature and strain rate can be formulated by incorporating the definition of the Zener-Hollomon parameters, and presented in the following Eq. 3:

$$Z = \dot{\varepsilon}\exp\left(\frac{Q}{RT}\right) \tag{3}$$

For determination of material constants (η, β, α, and n) can be directly achieved from experimental data collected through the hot compression test. The expressions presented have been derived from peak stress (σ_p) as referenced in previous works [8, 10, 11, 20-24]. By considering the low-stress level ($\alpha\sigma < 0.8$) and the high-stress level ($\alpha\sigma > 1.2$), plugging in the power law and the exponential law of $F(\sigma)$ into Eq. 1, the following equations are respectively derived as follows:

$$\dot{\varepsilon} = B\sigma_{p}^{\eta} \exp\left(-\frac{Q}{RT}\right) \tag{4}$$

$$\dot{\varepsilon} = \left(C\exp(\beta\sigma_{p})\right)\exp\left(-\frac{Q}{RT}\right) \tag{5}$$

and applying natural logarithms to both sides of Eq. 4 and Eq. 5, respectively, it can be written as:

$$\ln(\dot{\varepsilon}) = \ln(B) + \eta\ln(\sigma_{p}) - \frac{Q}{RT} \tag{6}$$

$$\ln(\dot{\varepsilon}) = \ln(C) + \beta\sigma_{p} - \frac{Q}{RT} \tag{7}$$

By keeping the temperature constant and considering the activation energy as a fixed parameter, taking partial differentiation of Eq. 6 and Eq. 7 respectively yields the parameter defined as follows:

$$\frac{1}{\eta} = \left[\frac{\partial\ln(\sigma_{p})}{\partial\ln(\dot{\varepsilon})}\right]_{T} \tag{8}$$

$$\frac{1}{\beta} = \left[\frac{\partial(\sigma_{p})}{\partial\ln(\dot{\varepsilon})}\right]_{T} \tag{9}$$

Through the use of the linear regression method, the material constants can be computed. The respective slopes of the fitting lines depicted in Figures 2(a) and 2(b), which are associated with the plots of $\ln(\sigma_p) - \ln(\dot{\varepsilon})$ and $\sigma_p - \ln(\dot{\varepsilon})$, yield the values of $1/\eta$ and $1/\beta$. The calculated average values of η and β were respectively 11.460 and 0.11885. Additionally, the value of α is found to be 0.010371. The utilization of the hyperbolic sine law of $F(\sigma)$ is an appropriate approach in characterizing the hot deformation behavior across a wide spectrum of stress levels [11, 21, 23]. By integrating the hyperbolic sine law (Eq. 2) into Eq. 1, then Eq. 1 is represented as follows:

$$\dot{\varepsilon} = A\left[\sinh(\alpha\sigma_{p})\right]^{n} \exp\left(-\frac{Q}{RT}\right) \tag{10}$$

The application of natural logarithms to both sides leads to the derivation of Eq. 10, as shown below:

$$\ln(\dot{\varepsilon}) = \ln(A) + n\ln[\sinh(\alpha\sigma_{p})] - \frac{Q}{RT} \tag{11}$$

By performing partial differentiation of Eq. 11, the apparent thermal activation energy Q under high temperature can be expressed as follows:

$$Q = R\left[\frac{\partial\ln(\dot{\varepsilon})}{\partial\ln[\sinh(\alpha\sigma_{p})]}\right]_{T}\left[\frac{\partial\ln[\sinh(\alpha\sigma_{p})]}{\partial(1/T)}\right]_{\dot{\varepsilon}} \tag{12}$$

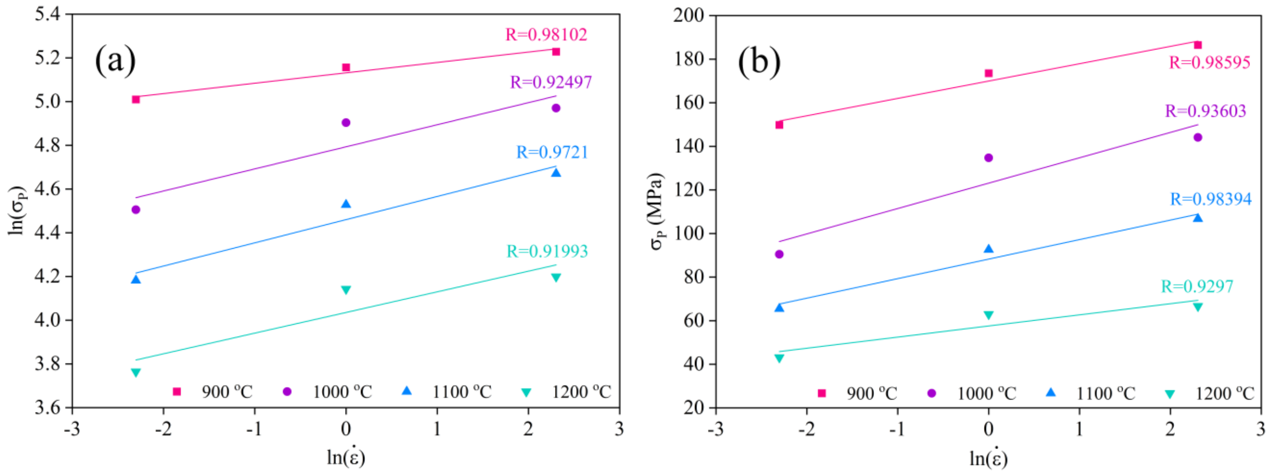

Figure 2 Plots of between (a) ln σ_p versus ln $\dot{\varepsilon}$ and (b) σ_p versus ln $\dot{\varepsilon}$ for calculation of hot working constants.

According to Eq. 12, the Q are derived from the slopes of the fitted lines in the scatter plots of $\ln[\sinh(\alpha\sigma_p)] - \ln(\dot{\varepsilon})$ and $\ln[\sinh(\alpha\sigma_p)] - 1/T$ in Figure 3(a) and Figure 3(b), respectively. Therefore, the average value of Q can be calculated as 608.97 kJ per mol.

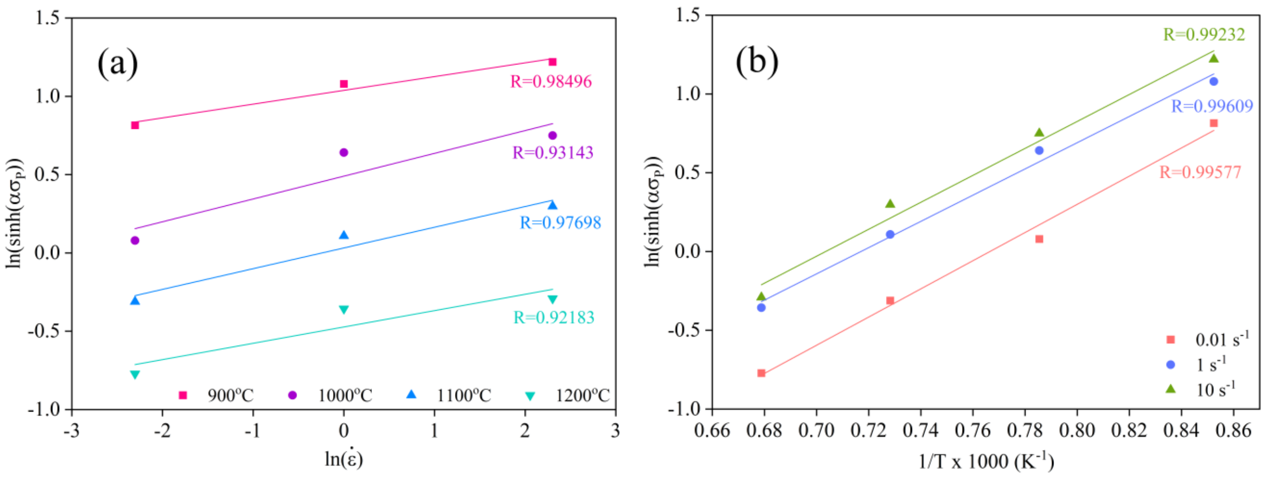

Figure 3 Plots of (a) $\ln[\sinh(\alpha\sigma_p)]$ against $\ln(\dot{\varepsilon})$ and (b) $\ln[\sinh(\alpha\sigma_p)]$ versus 1/T for calculation of the apparent thermal activation energy

By employing Eq.1, Eq. 2 and Eq. 3 as shown in Eq. 13, it is feasible to obtain the correlation throughout Z parameter and flow stress. Additionally, by applying the natural logarithms to both sides of Eq. 13, a new equation can be stated as Eq. 14:

$$Z = A[\sinh(\alpha\sigma_p)]^n = \dot{\varepsilon}\exp\left(\frac{Q}{RT}\right) \tag{13}$$

$$\ln(Z) = \ln(A) + n\ln[\sinh(\alpha\sigma_p)] \tag{14}$$

The scatter plot of $\ln(Z) - \ln[\sinh(\alpha\sigma_p)]$ displayed in Figure 4 demonstrate a good linear correlation, indicating a good fit. The intercept and slope of $\ln(Z) - \ln[\sinh(\alpha\sigma_p)]$ plot correspond to the values of A and n, which are calculated as 1.71099×10^{23} and 8.5106, respectively. Furthermore, it has been observed that the $\ln(Z)$ reduces as temperature rises and strain rate decreases. According to Eq. 13, it becomes practical to provide a description of the flow stress at a particular strain in terms of the Z parameter. This consideration takes into account the definition of the hyperbolic sine law, which may be seen below.

$$\sigma_p = \frac{1}{\alpha}\sinh^{-1}\left(\frac{Z}{A}\right)^{\frac{1}{n}} \tag{15}$$

$$\sigma_p = \frac{1}{\alpha}\sinh^{-1}\left(\frac{1}{A}\cdot\dot{\varepsilon}\cdot\exp\left(\frac{Q}{RT}\right)\right)^{\frac{1}{n}} \tag{16}$$

The inverse hyperbolic function was defined as follows:

$$\sinh^{-1}\left[(Z/A)^{\frac{1}{n}}\right] = \ln\left[(Z/A)^{\frac{1}{n}} + \left((Z/A)^{\frac{2}{n}} + 1\right)^{\frac{1}{2}}\right] \tag{17}$$

Substituting Eq.17 into Eq. 15, renders the flow stress in the form of Z parameter as:

$$\sigma_p = \frac{1}{\alpha}\ln\left\{(Z/A)^{\frac{1}{n}} + \left[(Z/A)^{\frac{2}{n}} + 1\right]\right\}^{\frac{1}{2}} \tag{18}$$

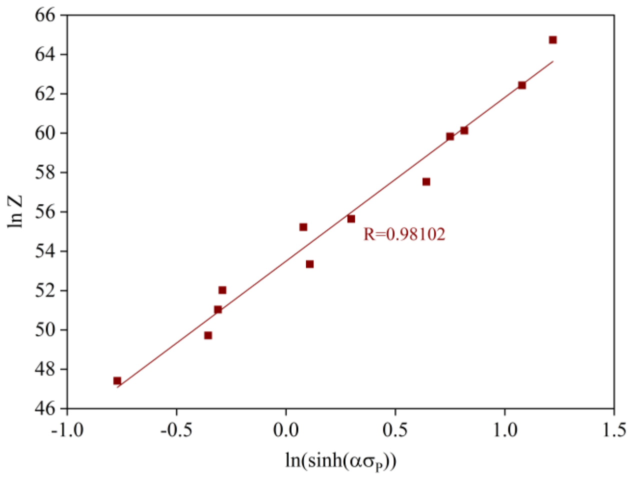

Figure 4 Plots of $\ln Z$ versus $\ln[\sinh(\alpha\sigma_p)]$ used to propose the constitutive equation

By utilizing general expressions, the peak stresses values of BS 080M46 medium carbon steel can be derived within the temperature range of 900°C to 1200°C and strain rates of 0.1, 1, and 10 s^{-1} by plugging the values of α, A, n, and Q into the constitutive model equations, specifically Eq. 16 and Eq. 18.

$$\sigma_p = \frac{1}{0.010371}\sinh^{-1}\left(\frac{1}{1.71099\times 10^{23}}\cdot\dot{\varepsilon}\cdot\exp\left(\frac{608.97\times 10^3}{RT}\right)\right)^{\frac{1}{8.5106}} \quad (19)$$

$$\sigma_p = \frac{1}{0.010371}\ln\left\{\left(\frac{Z}{1.71099\times 10^{23}}\right)^{\frac{1}{8.5106}} + \left[\left(\frac{Z}{1.71099\times 10^{23}}\right)^{\frac{2}{8.5106}} + 1\right]^{\frac{1}{2}}\right\} \quad (20)$$

3.3 Hansel-Spittel Constitutive model

To investigate the deformation behavior BS 080M46 medium carbon steel, the Hansel-Spittel was developed. This model is designed to represent the dependence of flow stress (σ), temperature (T), strain (ε) and strain rate ($\dot{\varepsilon}$) [6, 15-18]. The Hansel-Spittel model is then utilized to simulate the deformation behavior during metal forming processes and optimize the manufacturing process. The mathematical expression of flow stress can be written as follows:

$$\sigma = Ae^{m_1 T}\varepsilon^{m_2}\dot{\varepsilon}^{m_3}e^{\frac{m_4}{\varepsilon}}(1+\varepsilon)^{m_5 T}e^{m_7\varepsilon}\dot{\varepsilon}^{m_8 T}T^{m_9} \quad (21)$$

The model, as indicated by Eq. 21, is composed of nine parameters. Among these parameters, A represents the material constant while m_1, m_2, m_3, m_4, m_5, m_7, m_8, and m_9 signify the material parameters, as has been previously established in sources [6, 14, 18, 17, 25]. The temperature correlation coefficient is denoted by m_1, whereas m_9 indicates the temperature-strengthening index. The sensitivity of the material to strain is determined by m_2, m_4, and m_7. The coefficient m_3 is associated with the sensitivity of the material to strain rate. The material parameter m_5 represents the coefficient of coupling between temperature and strain, while m_8 is the coefficient of coupling between strain rate and temperature. By applying the natural logarithm to the both sides of the Eq. 21, as demonstrated by Eq. 22:

$$\ln(\sigma) = \ln(A) + m_1 T + m_2\ln(\varepsilon) + m_3\ln(\dot{\varepsilon}) + \frac{m_4}{\varepsilon} + m_5 T\ln(1+\varepsilon) + m_7\varepsilon + m_8 T\ln(\dot{\varepsilon}) + m_9\ln(T) \quad (22)$$

When the strain (ε) and temperature (T) are maintained at fixed vales, the following expression of K_1 remains constant:

$$K_1 = \ln(A) + m_1 T + m_2\ln(\varepsilon) + \frac{m_4}{\varepsilon} + m_5 T\ln(1+\varepsilon) + m_7\varepsilon + m_9\ln(T) \quad (23)$$

Then Eq. 22 can be transformed as follows:

$$\ln(\sigma) = (m_3 + m_8 T)\ln(\dot{\varepsilon}) + K_1 \quad (24)$$

For constant temperature (900°C), the scatter diagram (Figure 5(a)) of $\ln(\sigma)$ and $\ln(\varepsilon)$ was plotted and the linear regression was performed to determine the values of m_3+m_8T and K_1. In Figure 5(b), the linear relationship between m_3+m_8T and the temperature under varying strain is depicted, where the slope corresponds to m_8 and the intercept corresponds to the average value of m_3. Therefore, the average values of m_3 and m_8 are -0.12044 and 0.00021, respectively. The average correlation coefficients (R) for the $m_3+m_8T - K_1$ plots at 900°C, 1000°C, 1100°C, and 1200°C are 0.92218, 0.86920, 0.94339, and 0.91639, respectively. The overall average R is calculated to be 0.91279. Additionally, the average R for the $m_3+m_8T - T$ plots is 0.81099. The linear regression analysis of the $m_3+m_8T - K_1$ and $m_3+m_8T - T$ plots indicates a relatively weak correlation between the fitted regression lines and the data points. The poor correlation observed in the curve fitting of the $m_3+m_8T - K_1$ plot and $m_3+m_8T - T$ plots can indeed affect the accuracy of the average values of m_3 and m_8.

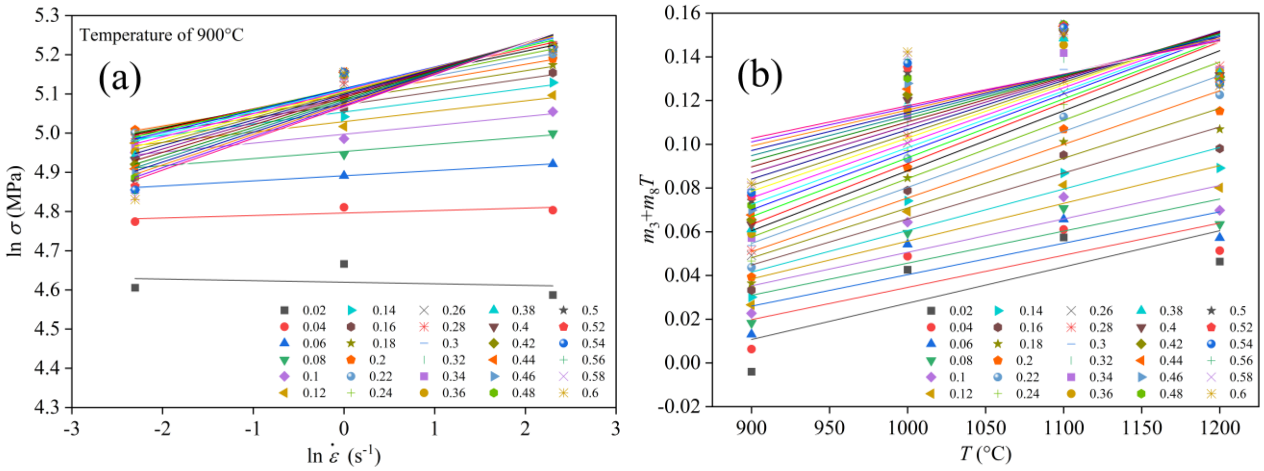

Figure 5 (a) Linear regression analysis of (a) $\ln(\sigma)$ against $\ln(\dot{\varepsilon})$ plot at temperature of 900°C and (b) $m_3 + m_8T$ versus T under different strain

The expression of K_2 remains constant when the both strain (ε) and strain rate $(\dot{\varepsilon})$ are held at fixed values, as illustrated by the equation below:

$$K_2 = \ln(A) + m_2\ln(\varepsilon) + m_3\ln(\dot{\varepsilon}) + \frac{m_4}{\varepsilon} + m_7\varepsilon + m_8T\ln(\dot{\varepsilon}) \tag{25}$$

Hence, Eq. 22 can be modified into:

$$\ln(\sigma) = K_2 + [m_1 + m_5\ln(1+\varepsilon) + m_8\ln(\dot{\varepsilon})]T + m_9\ln(T) \tag{26}$$

In this case, $k = m_1 + m_5\ln(1+\varepsilon) + m_8\ln(\dot{\varepsilon})$ is set. The function form of $y = K_2 + kx + m_9\ln(x)$ can be fitted to obtain the value of m_9 for all strain rates. The average value for m_9 is 5.26228. The Figures 6(a) and 6(b) display the examples of the fitted curve for the scatter plot of $\ln(\sigma) - T$ are at strain rate of 0.1 s^{-1} and 1 s^{-1}, respectively. When the strain rate is kept fixed, the data can be fitted with formula $k = K_3 + m_5\ln(1+x)$, where $K_3 = m_1 + m_8\ln(\dot{\varepsilon})$, under various strain conditions. The values m_5 and m_1 are -0.00865 and -0.00655, respectively.

When maintaining a constant strain rate $(\dot{\varepsilon})$ and temperature, the following expression of K_4 remains constant:

$$K_4 = \ln(A) + m_1T + m_3\ln(\dot{\varepsilon}) + m_8T\ln(\dot{\varepsilon}) + m_9\ln(T) \tag{27}$$

Thus, Eq. 22 can be turned into:

$$\ln(\sigma) = m_2\ln(\varepsilon) + \frac{m_4}{\varepsilon} + m_5T\ln(1+\varepsilon) + m_7\varepsilon + K_4 \tag{28}$$

At specific temperatures, the function $y = m_2\ln x + (m_4/x) + m_5T\ln(1+x) + m_7x + K_4$ is applied to the scatter plots of $\ln(\sigma)$ versus ε, and the example of resulting regression curves at temperature of 900°C and 1100°C are illustrated in Figures 7(a) and 7(b), respectively. The average values of m_2, m_4 and m_7 were calculated for all temperature conditions, yielding the following results are: m_2 = 0.40839, m_4 = 0.00210 and m_7 = 2.6322.

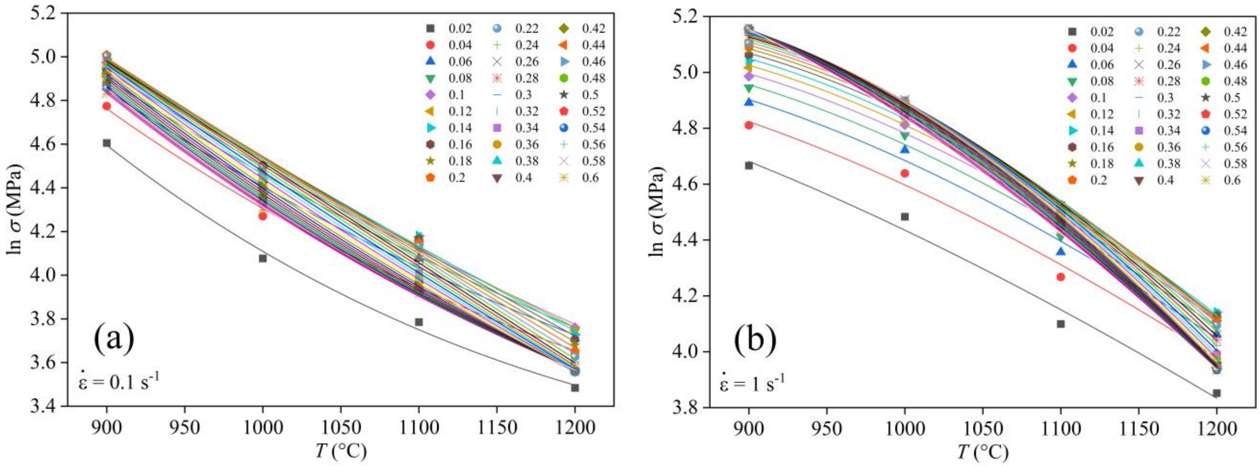

Figure 6 $\ln(\sigma) - T$ fitting curves at strain rate of (a) 0.1 s^{-1} and (b) 1 s^{-1}

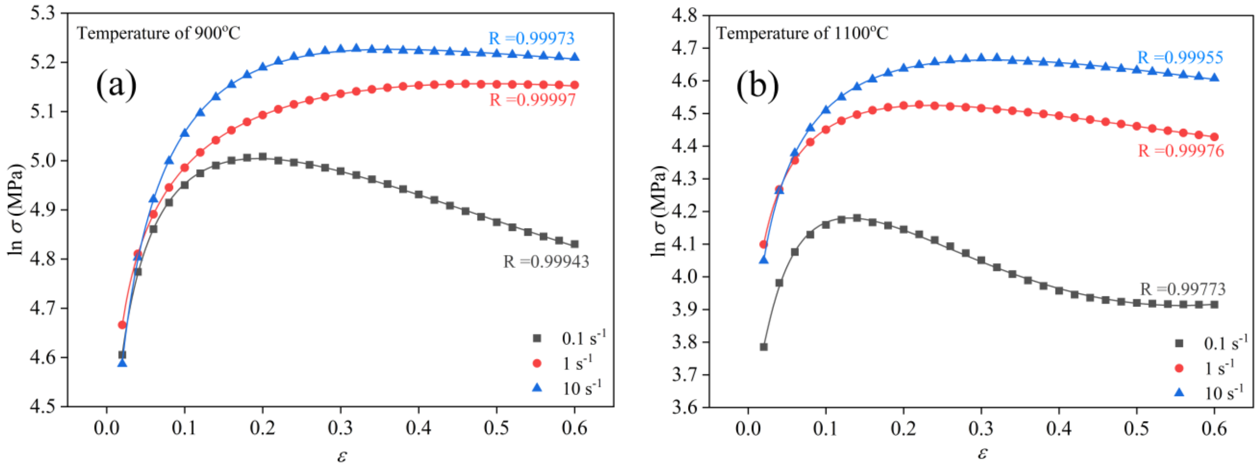

Figure 7 Relationships of $\ln(\sigma) - \varepsilon$ at temperature of (a) 900°C and (b) 1100°C

The value of A can be calculated by plugging the values of m_1, m_2, m_3, m_4, m_5, m_7, m_8 and m_9 into Eq. 21. By performing this calculation, the value of A can be determined, with an average value of A is 0.00121. Upon substituting of the values obtained for the aforementioned parameters into Eq. 21, the constitutive equation of BS 080M46 medium carbon steel can be formulated as presented below:

$$\sigma = 0.00121 e^{-0.00655T} \varepsilon^{0.40839} \dot{\varepsilon}^{-0.12044} e^{\frac{0.00210}{\varepsilon}} (1+\varepsilon)^{-0.00865T} e^{2.6322\varepsilon} \dot{\varepsilon}^{0.00021T} T^{5.26228} \tag{29}$$

4. Verification of the developed constitutive models

In an effort for verifying the precision of the constitutive models, an analysis was conducted to compare the flow stresses predicted by the models and those obtained experimentally. Figure 8 displays the flow stress curves predicted by the models along with the experimental results for BS 080M46 medium carbon steel for entire test conditions. It is observable that the predicted flow stresses, exhibit a good accordance with the corresponding experimental stress-strain data. To assess the reliability and precision of the developed constitutive models at high temperatures, three statistical parameters, specially the average absolute relative error (*AARE*), root mean square (*RMS*) and correlation coefficient (*R*) were employed, following the approaches in previous studies [6, 14, 15, 18]. The formulas for these parameters were as belows:

$$AARE = \frac{1}{N}\sum_{i=1}^{N}\left|\frac{E_i - P_i}{E_i}\right| \times 100 \tag{30}$$

$$RMS = \sqrt{\frac{1}{N}\sum_{i=1}^{N}(E_i - P_i)^2} \tag{31}$$

$$R = \frac{\sum_{i=1}^{N}(E_i - \bar{E})(P_i - \bar{P})}{\sqrt{\sum_{i=1}^{N}(E_i - \bar{E})^2 \sum_{i=1}^{N}(P_i - \bar{P})^2}} \tag{32}$$

The given equation, from Eq. 30 to Eq. 32, serves to relate the experimental value (*E*) with the predicted value (*P*), where *N* represents the total number of data points considered for this investigation. $\bar{E}$ and $\bar{P}$ represent, correspondingly, the average values of *E* and *P*. The statistical parameter denoted as the average absolute relative error, *AARE*, measures the average deviation, expressed as a percentage. It offers an indicator of the overall accuracy of the predictions across the dataset. The standard deviation of the predicted value from the corresponding experimental value is represented by the root mean square error, *RMS*. This parameter provides an evaluation of the dispersion or spread of the predictions around the experimental data points. The correlation coefficient, *R*, assesses the linearity between predicted and experimental values. A value of *R* in close proximity to 1 suggests a strong linear relationship, approaching a perfect match between predicted and experimented values. Figures 9(a) and 9(b), respectively, illustrates experimental values plotted against predicted values obtained from the Arrhenius-based and the Hansel-Spittel constitutive model. In Figure 9(c), the *AARE* is presented in the bar graph with the values, indicating the level of accuracy achieved by both developed constitutive models in predicting flow stress. The calculation of *AARE* for specific conditions involves Eq. 30 for each set of deformation conditions: 900°C, 1000°C, 1100°C, and 1200°C, each subjected to strain rates of 0.1 s^{-1}, 1 s^{-1}, and 10 s^{-1} under each of the developed constitutive models. Subsequently, the *AARE* values obtained for each deformation condition are averaged, followed by the computation of an overall average. For the Arrhenius-based constitutive model, the maximum relative error is 15.7618% at a strain rate of 1 s^{-1} and a temperature of 1000°C. Conversely, the minimum relative error is 1.6924% at a strain rate of 0.1 s^{-1} and a temperature of 1000°C. For the Hansel-Spittel constitutive model, the maximum relative error is 14.2316% at a strain rate of 1 s^{-1} and a temperature of 1000°C, while the minimum relative error is 3.8399% at a strain rate of 1 $s^{-1}$and a temperature of 900°C. When evaluating the performance of constitutive models, it's important to consider all three statistical parameters (*AARE*, *RMS* and *R*).-From Figure 9, The Arrhenius-based model yields an *AARE* of 7.5231%, an *RMS* of 7.3565 MPa, and an *R* value of 0.98450, while the Hansel-Spittel model achieves an *AARE* of 9.0647%, an *RMS* of 9.1400 MPa, and an *R* value of 0.98016. By considering each statistical parameters, suggest that Arrhenius-based model provides a higher level of precision and reliable prediction of flow stress compared to the Hansel-Spittel model.

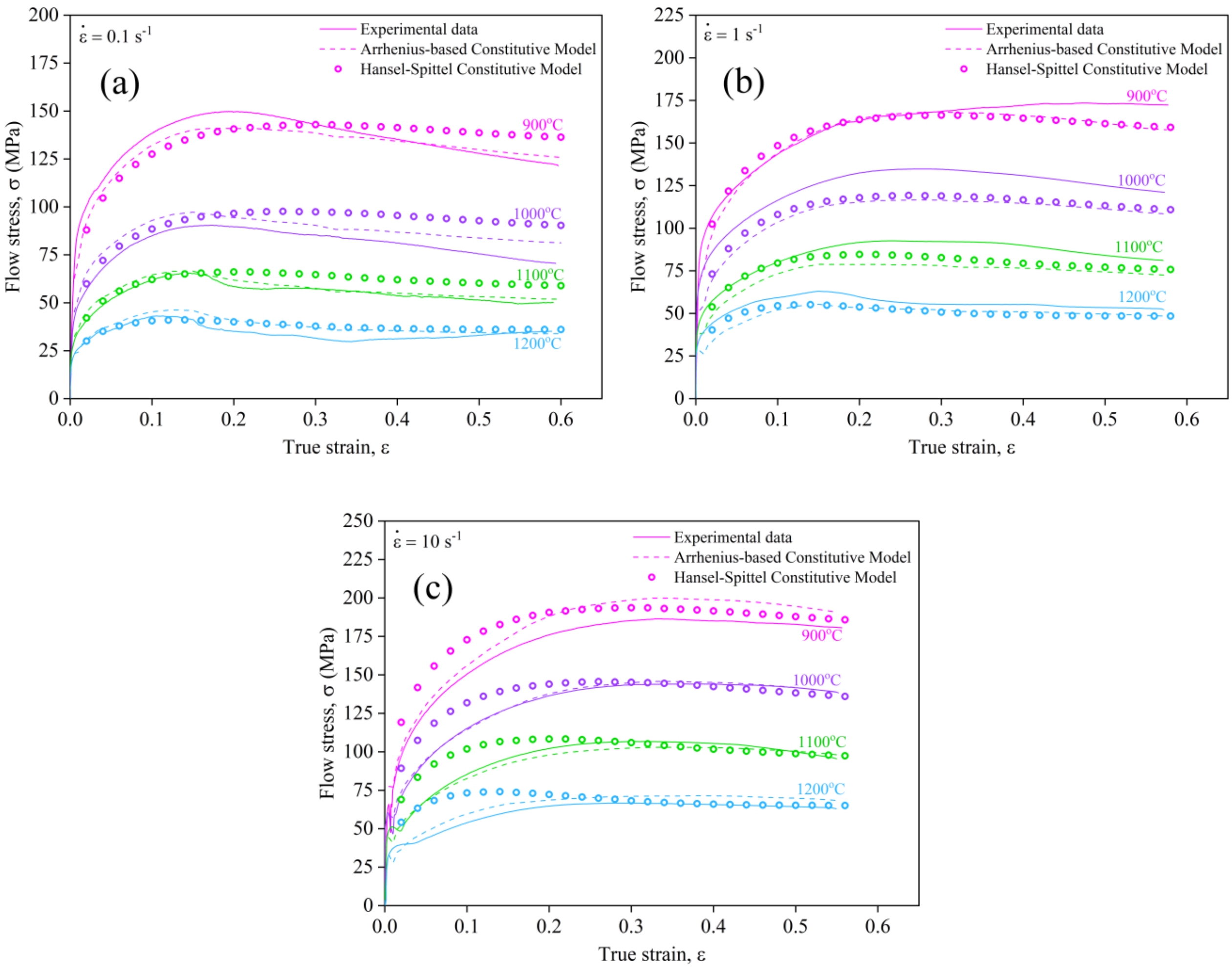

Figure 8 Comparing the predicted flow curves of 080M46 medium carbon steel with the experimental flow curves, which vary with deformation temperature at (a) 0.1 s^{-1} (b) 1 s^{-1} and (c) 10 s^{-1}.

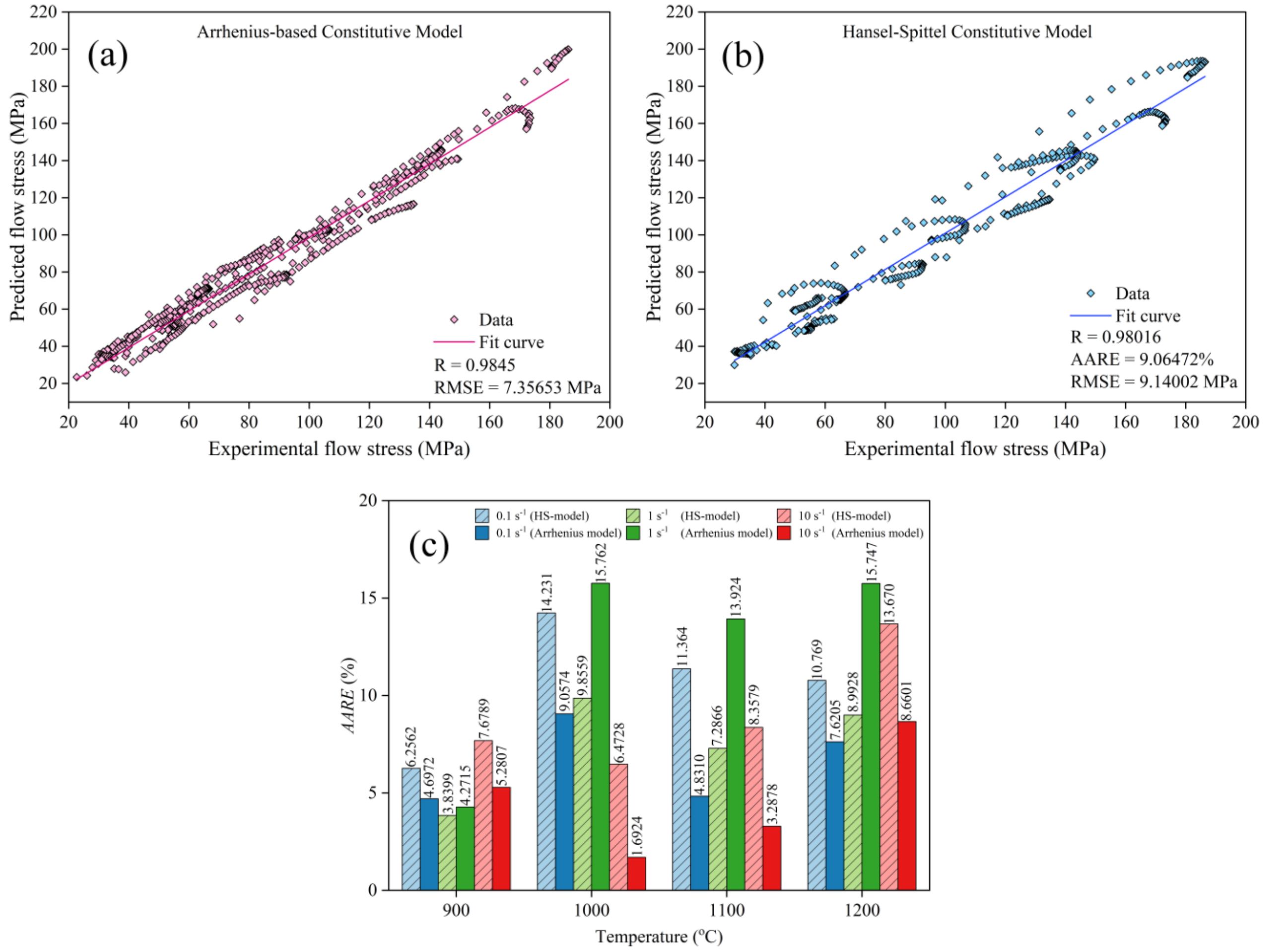

Figure 9 Correlation between the experimental and predicted flow stress from (a) Arrhenius-based and (b) Hansel-Spittel constitutive model, along with (c) *AARE* (%) evaluation.

For validation the developed Arrhenius-based and Hansel-Spittle constitutive model in finite element modeling, both developed constitutive models were implemented into finite element software QFORM 10.1.6. Tetrahedral elements were used to create the elements of the finite element (FE) model (Figure 10(a)). In the simulation setup, the cylindrical billet was designated as a deformable body, however the tools were defined as rigid bodies. This approach allows for the analysis of the deformation behavior of the sample under the applied loads, while the tools remain fixed and unaffected by the simulation, ensuring their stability and immobility throughout the process. The processing conditions have been set in conformity with the actual experimental conditions. A total of twelve sets of deformation conditions were selected to simulate the hot compression test. As illustrated in Figure 10(b), the load-displacement curves obtained through FE simulation using both developed models conform to the experimental load-displacement curves [14, 15]. The average error observed for the developed Hansel-Spittel model is 2.8400%, while the developed Arrhenius-based model exhibits an average error of 5.2560%. The validation of the accuracy of both developed constitutive models for BS 080M46 medium carbon steel was indeed based on the small errors observed when comparing the simulated results to the corresponding experimental data. These small errors indicate a significant level of accuracy and confirm the reliability of the developed models in predicting the flow behavior of BS 080M46 medium carbon steel during hot compression tests.

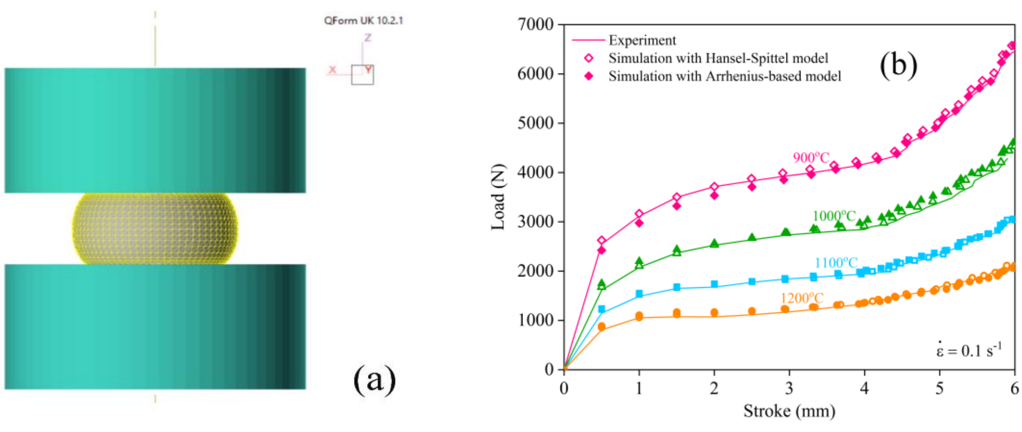

Figure 10 (a) 3D-FE model for hot compression test and (b) load versus displacement from experiment and simulation at strain rate of (b) 0.1 s^{-1}, (c) 1 s^{-1} and (d) 10 s^{-1}.

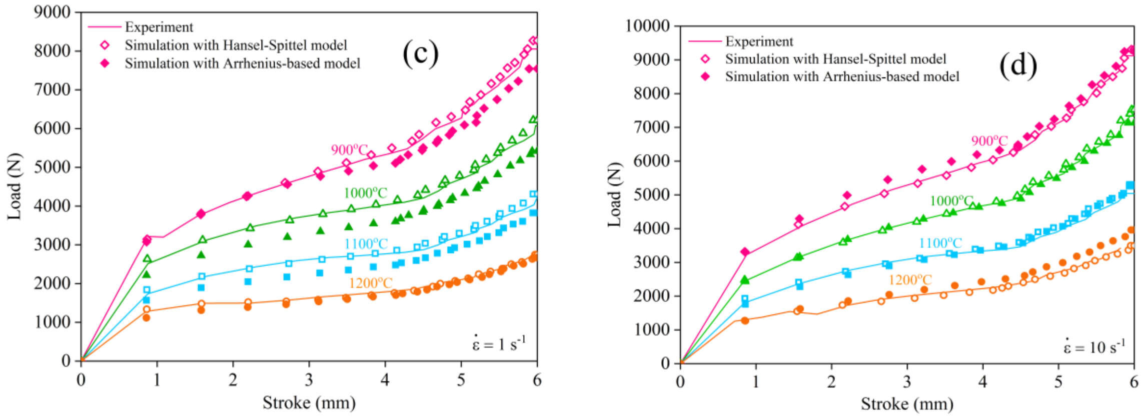

Figure 10 (continued) (a) 3D-FE model for hot compression test and (b) load versus displacement from experiment and simulation at strain rate of (b) 0.1 s^{-1}, (c) 1 s^{-1} and (d) 10 s^{-1}.

5. Conclusion

In this study, hot compression tests were performed on a dilatometer at temperatures ranging from 900 to 1200°C, and applying strain rates of 0.1, 1, and 10 s^{-1} for BS 080M46 medium carbon steel. To precisely predict the flow behavior under high temperatures, two constitutive models were developed: the Arrhenius-based model and the Hansel-Spittel model, taking into account the effect of strain, strain rate, and deformation temperature on the flow stress. Both the Arrhenius-based and Hansel-Spittel models were subjected to verification through the calculation of three statistical parameters: average absolute relative error (*AARE*), root mean square error (*RMS*), and correlation coefficient (*R*). The findings indicated that both the Arrhenius-based and the Hansel-Spittel constitutive models were successful in accurately predicting the flow stress of BS 080M46 steel under various deformation conditions. In comparison to the Hansel-Spittel constitutive model, the developed Arrhenius-based model demonstrated superior accuracy and reliability in its predictive capabilities, yielding an *AARE* of 7.5231%, an *RMS* of 7.3565 MPa, and an *R* value of 0.98450. The findings suggest that the Arrhenius-based model provide more accuracy and precise prediction of the flow stress for BS 080M46 medium carbon steel. The accuracy and reliability of the constitutive models in predicting the flow stress of BS 080M46 medium carbon steel under high temperature conditions have been validated through load-displacement curve comparisons, where the obtained curves from hot compression tests and FE simulations were compared. The successful comparison of these curves further confirms their reliability and suitability of the constitutive models for effectively predicting flow stress under high-temperature conditions. The future scope of this study may extend to the evolution of microstructure for the hot compression experiment. This can be achieved by using appropriate constitutive models and incorporating detailed microstructural information in finite element simulations**.** These approaches aim to advance the understanding of material behavior in hot compression experiments.

6. Acknowledgement

The authors would like to express their gratitude for the financial support received through the Petchra Pra Jom Klao Ph.D. Research Scholarship (KMUTT-NSTDA) from King Mongkut's University of Technology Thonburi. Additionally, they extend their sincere appreciation to S.B.-CERA Co., Ltd. for sharing their technical knowledge and providing assistance with the industrial parts.

7. References

[1] Jantepa N, Suranuntchai S. Investigation of hot deformation behavior of SNCM8 alloy steel. World J Mech. 2021;11(3):17-33.
[2] Altan T, Ngaile G, Shen G. Cold and hot forging: fundamentals and applications. Materials Park: ASM International; 2004.
[3] Siripath N, Suranuntchai S, Sucharitpwatskul S. Cylindrical billet size optimization for hot closed-die forging of the upper ball joint. Key Eng Mater. 2023;946:9-14.
[4] Patnamsetty M, Saastamoinen A, Somani MC, Peura P. Constitutive modelling of hot deformation behaviour of a CoCrFeMnNi high-entropy alloy. Sci Technol Adv Mater. 2020;21(1):43-55.
[5] Prasad YVRK, Rao KP, Sasidhar S. Hot Working guide: a compendium of processing maps. 2nd ed. Materials Park: ASM International; 2015.
[6] Liang Q, Liu X, Li P, Ding P, Zhang X. Development and application of high-temperature constitutive model of HNi55-7-4-2 Alloy. Metals. 2020;10(9):1250.
[7] Sellars CM, McTegart WJ. On the mechanism of hot deformation. Acta Metallurgica. 1966;14(9):1136-8.
[8] Kumar N, Kumar S, Nath SK. Determination of Zener-Hollomon parameter of a low alloy medium carbon steel under hot compression physical simulation. Proceedings of the 4th International Conference on Thermo-mechanical Simulation and Processing of Steels (SimPro 16); 2016 Feb 10-12; Ranchi, India. p. 346-52.
[9] Li HZ, Zhang XM, Chen MG, Liu Y, Gao H. Hot deformation behavior of 2519 Al alloy during isothermal compression. Mater Sci Forum. 2007;546-549:749-54.
[10] Xiao ZB, Wang Q, Huang YC, Hu J, Li M. Hot deformation characteristics and processing parameter optimization of Al–6.32Zn–2.10Mg alloy using constitutive equation and processing map. Metals. 2021;11(2):360.
[11] Dandekar TR, Khatirkar RK, Gupta A, Bibhanshu N, Bahdauria A, Suwas S. Strain rate sensitivity behaviour of Fe–21Cr-1.5Ni–5Mn alloy and its constitutive modelling. Mater Chem Phys. 2021;271:124948.
[12] Yin F, Hua L, Mao H, Han X. Constitutive modeling for flow behavior of GCr15 steel under hot compression experiments. Mater Des. 2013;43:393-401.

[13] Hansel A, Spittel T. Kraft- und Arbeitsbedarf bildsamer Formgeburgsverfahren. Leipzig: VEB DeutscherVerlag fur Grundstoffindustrie; 1978. (In German)
[14] Chen X, Wang N, Ma X, Zhou H. Hot deformation behaviour and Hansel-Spittel constitutive model of Cr5 alloy for heavy backup roll. Int J Comput Mater Sci Surf Eng. 2018;7(3/4):205-17.
[15] Chen X, Du Y, Du K, Lian T, Liu B, Li Z, et al. Identification of the constitutive model parameters by inverse optimization method and characterization of hot deformation behavior for ultra-supercritical rotor steel. Materials. 2021;14(8):1958.
[16] Cyganek Z, Tkocz M. The effect of AZ31 alloy flow stress descriotion on the accuracy of forward extrusion fe simulation results. Arch Metall Mater. 2012;57(1):199-204.
[17] Chadha K, Shahriari D, Jahazi M. An approach to develop hansel–spittel constitutive equation during ingot breakdown operation of low alloy steels. In: Muruganant M, Chirazi A, Raj B, editors. Frontiers in Materials Processing. Applications, Research and Technology. Singapore: Springer; 2018. p. 239-46.
[18] Chen X, Lian T, Zhang B, Du Y, Du K, Liu B, et al. The parameters identification of high-temperature constitutive model based on inverse optimization method and 3D processing map of Cr8 alloy steel. Materials. 2021;14(9):2216.
[19] Sanrutsadakorn A, Uthaisangsuk V, Suranuntchai S, Thossatheppitak B. Constitutive modeling of flow behaviour of AISI 4340 steel under hot working conditions. Appl Mech Mater. 2013;249-250:863-9.
[20] Sanrutsadakorn A, Uthaisangsuk V, Suranuntchai S, Thossatheppitak B. Investigation of hot deformation characteristics of AISI 4340 steel using processing map. Adv Mater Res. 2013;683:301-6.
[21] Thossatheppitak B, Uthaisangsuk V, Mungsuntisuk P, Suranuntchai S, Manonukul A. Flow behaviour of Nickel Aluminium Bronze under hot deformation. Mater Sci Eng A. 2014;604:183-90.
[22] Aungsusiripong A, Suranuntchai S, Uthaisangsuk V. Constitutive modeling of flow stress of MAB alloy. Adv Mater Res. 2015;1101:442-5.
[23] Banerjee S, Robi PS, Srinivasan A, Kumar LP. High temperature deformation behavior of Al–Cu–Mg alloys micro-alloyed with Sn. Mater Sci Eng A. 2010;527(10-11):2498-503.
[24] Wang M, Li Y, Wang W, Zhou J, Chiba A. Quantitative analysis of work hardening and dynamic softening behavior of low carbon alloy steel based on the flow stress. Mater Des. 2013;45:384-92.
[25] Chen X, Zhang B, Du Y, Liu M, Bai R, Si Y, et al. Constitutive model parameter identification based on optimization method and formability analysis for Ti6Al4V alloy. Materials. 2022;15(5):1748.